The TWD40-2 protein and the AP2 complex cooperate in the clathrin-mediated endocytosis of cellulose synthase to regulate cellulose biosynthesis

Logan Bashline, Shundai Li, Xiaoyu Zhu, and Ying Gu[1]

Center for Lignocellulose Structure and Formation, Department of Biochemistry and Molecular Biology, Pennsylvania State University, University Park, PA 16802

Edited by Natasha V. Raikhel, Center for Plant Cell Biology, Riverside, CA, and approved September 3, 2015 (received for review May 13, 2015)

Cellulose biosynthesis is performed exclusively by plasma membrane-localized cellulose synthases (CESAs). Therefore, the trafficking of CESAs to and from the plasma membrane is an important mechanism for regulating cellulose biosynthesis. CESAs were recently identified as cargo proteins of the classic adaptor protein 2 (AP2) complex of the clathrin-mediated endocytosis (CME) pathway. The AP2 complex of the CME pathway is conserved in yeast, animals, and plants, and has been well-characterized in many systems. In contrast, the recently discovered TPLATE complex (TPC), which is proposed to function as a CME adaptor complex, is only conserved in plants and a few other eukaryotes. In this study, we discovered that the TWD40-2 protein, a putative member of the TPC, is also important for the endocytosis of CESAs. Genetic analysis between TWD40-2 and AP2M of the AP2 complex revealed that the roles of TWD40-2 in CME are both distinct from and cooperative with the AP2 complex. Loss of efficient CME in *twd40-2-3* resulted in the unregulated overaccumulation of CESAs at the plasma membrane. In seedlings of *twd40-2-3* and other CME-deficient mutants, a direct correlation was revealed between endocytic deficiency and cellulose content deficiency, highlighting the importance of controlled CESA endocytosis in regulating cellulose biosynthesis.

cellulose synthase | endocytosis | clathrin | plasma membrane | trafficking

Cellulose is synthesized at the plasma membrane (PM) by large cellulose synthase (CESA) complexes (CSCs) that directly extrude the nascent cellulose polymers into the cell wall (1–3). Fluorescent protein fusions of CESA proteins (FP-CESAs) have been instrumental in advancing our understanding of cellulose biosynthesis (4, 5). The delivery of CSCs to the PM has been shown to coincide with the position of cortical microtubules (CMTs) that run along the cytoplasmic surface of the PM (6, 7). At the PM, CSCs are joined by cellulose synthase interactive (CSI1 and CSI3) proteins during cellulose biosynthesis that link the PM-localized CSCs to the CMTs and guide CSC motility, which is believed to be driven by cellulose biosynthesis, laterally in the plane of the PM in linear trajectories along CMTs (8–10). Plant cells contribute a great deal of energy not only to the biosynthesis of cellulose but also to the synthesis, assembly, distribution, and organization of CSCs (3). The prerequisite that CSCs must be localized to the PM to synthesize cellulose and that CSCs are both delivered to and travel along CMTs highlights the importance of coordinated CSC trafficking in the regulation of cellulose biosynthesis.

The organized and particulate distribution of FP-CESAs at the PM makes CESA an ideal model cargo protein for the investigation of trafficking pathways and mechanisms in *Arabidopsis* (3). In fact, we recently identified CESA as a bona fide cargo protein of the clathrin-mediated endocytosis (CME) pathway (11). In that study, we showed that the medium subunit of the heterotetrameric CME adaptor protein 2 (AP2) complex, AP2M (previously referred to as μ2), directly interacts with CESAs to mediate CESA endocytosis and that inefficient CESA endocytosis in *ap2m-1* (previously referred to as *μ2-1*) caused an increased density of FP-CESAs at the PM (11). Together, that study and others functionally characterized the existence of the AP2 complex in plants (11–15), which, in a wide variety of eukaryotes, acts as a central core in CME by docking to the PM and recruiting cargo proteins, clathrin cages, and other accessory proteins to the sites of CME (16). Recently, a series of coimmunoprecipitation experiments identified a new putative CME adaptor complex in plants, the TPLATE complex (TPC) (17). Subsequently, TPC components were shown to be partially or fully conserved in a few other eukaryotes, and have been speculated to represent the remnants of an evolutionarily ancient trafficking complex that existed in the last eukaryotic common ancestor (18). In *Arabidopsis*, many TPC mutations are lethal, but live-cell imaging and artificial knockdown of two TPC components, TML and TPLATE, have exposed a functional relationship between the TPC, AP2, and CME (17).

In the current study, a screen for mutants that exhibit short etiolated hypocotyls, a feature that is sometimes associated with cellulose deficiency, identified *SALK_112497*, which was named *twd40-2-3* because it is allelic to two mutants of TWD40-2, a putative member of the TPC. The previously identified *twd40-2-1* and *twd40-2-2* alleles have a male sterility phenotype that prevented functional characterization of TWD40-2 (17). Currently, the only evidence connecting TWD40-2 to the TPC or to CME is its ability to coimmunoprecipitate with TPC components (17). Therefore, the specific function of TWD40-2 remains uncharacterized, and it remains unknown whether the association between TWD40-2 and the TPC is permanent or transient. Homozygous *twd40-2-3* mutants are viable and propagable, which has enabled us to use functional genetics to investigate the role of TWD40-2 in endocytosis and to learn how defects in endocytosis interfere with cellulose biosynthesis through disrupting CESA trafficking.

Significance

Our study advances the understanding of how plants make cellulose, a critical constituent of the plant cell wall and the most abundant organic polymer in the terrestrial biosphere. Cellulose is synthesized at the plasma membrane by cellulose synthase (CESA) complexes. Here we highlight the importance of regulated CESA endocytosis in cellulose biosynthesis in *Arabidopsis*. Furthermore, we show that the TWD40-2 protein, a putative member of the TPLATE complex, functions in clathrin-mediated endocytosis (CME) in ways that are both distinct from and cooperative with the functionally conserved CME adaptor protein 2 (AP2) complex. Because the TPLATE complex of plants is not conserved in animals, our characterization of TWD40-2 offers the opportunity to provide insight into the evolution of eukaryotic trafficking machinery.

Author contributions: L.B., S.L., and Y.G. designed research; L.B., S.L., and X.Z. performed research; L.B., S.L., X.Z., and Y.G. analyzed data; and L.B. and Y.G. wrote the paper.

The authors declare no conflict of interest.

This article is a PNAS Direct Submission.

Freely available online through the PNAS open access option.

[1]To whom correspondence should be addressed. Email: yug13@psu.edu.

This article contains supporting information online at www.pnas.org/lookup/suppl/doi:10.1073/pnas.1509292112/-/DCSupplemental.

Results

***twd40-2-3* Was Isolated from a Short Etiolated Hypocotyl Screen and Shows a Genetic Interaction with *ap2m-1*.** A large pool of T-DNA insertion lines was screened for mutants that exhibited short etiolated hypocotyls. *twd40-2-3* not only displayed short etiolated hypocotyls but also had short roots in light-grown seedlings and dwarfed adult plants (Fig. 1 *A*–*D*). Although *twd40-2-3* is propagable, *twd40-2-1* and *twd40-2-2* were previously shown to be lethal due to a male sterility phenotype (17). To discern the nature of *twd40-2-3*, anti–TWD40-2 antibodies were raised against heterologously expressed TWD40-2 and used for Western blot analysis. Anti–TWD40-2 recognized a protein with an electrophoretic mobility that was slightly larger than the predicted molecular mass of TWD40-2 of ∼150 kDa (Fig. 1*E*). TWD40-2 protein expression was specifically knocked down, but not nullified, in *twd40-2-3*, which may explain the viability of *twd40-2-3* mutants (Fig. 1*E*). To understand the transcriptional influence of *twd40-2-3*, real-time quantitative (q)PCR analysis was performed with primer pairs upstream (UP) and downstream (DN) of the T-DNA insertion site (Fig. S1 *A* and *C*). In *twd40-2-3*, UP primers indicated normal levels of *TWD40-2* expression but DN primers indicated an approximate 60% reduction in *TWD40-2* expression (Fig. S1*C*), suggesting that incomplete TWD40-2 transcripts exist in *twd40-2-3*. Furthermore, RT-PCR with a primer set that flanks the T-DNA insertion site (P2) amplified a knocked-down level of *TWD40-2* transcripts in *twd40-2-3*, which suggests that the T-DNA can be spliced out of some *TWD40-2* transcripts in *twd40-2-3* (Fig. S1 *B* and *D*).

To gain insight into the function of TWD40-2, a construct containing GFP-TWD40-2 driven by its native promoter was transformed into *twd40-2-3*, which rescued the growth defects of *twd40-2-3* (Fig. S2 *A*–*C*). As expected, Western blot analysis of GFP-TWD40-2 *twd40-2-3* seedlings showed knocked-down expression of endogenous TWD40-2 and a mobility-shifted protein of increased molecular mass corresponding to GFP-TWD40-2 (Fig. 1*E*). In epidermal cells of etiolated hypocotyls, GFP-TWD40-2 localized exclusively to discrete foci at the PM that exhibited appearing and disappearing behavior that was reminiscent of previously observed components of the CME pathway including clathrin light chain (CLC), AP2M, the sigma subunit of the AP2 complex (AP2S), and dynamin related proteins (DRPs) (11, 13, 19), suggesting that TWD40-2 might also be involved in endocytosis (Fig. S2*D*).

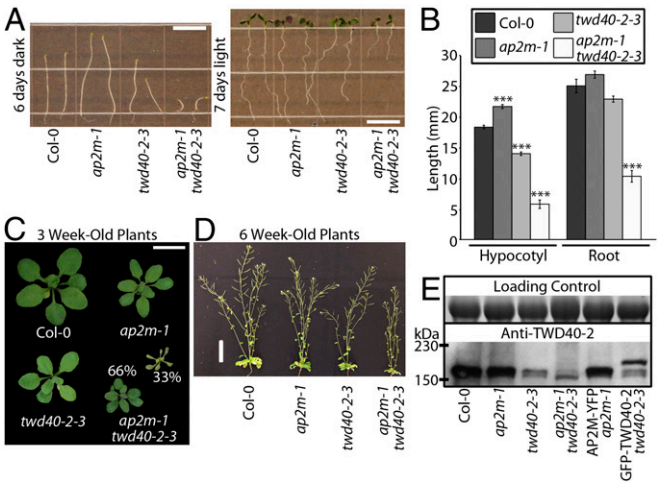

Fig. 1. *twd40-2-3* is a knockdown allele that exhibits dwarf phenotypes and shows a genetic interaction with *ap2m-1*. (*A* and *B*) The length of etiolated seedlings and light-grown seedling roots was measured. (Scale bars, 10 mm.) Error bars are SEM. ***$P < 0.0001$ ($10 \leq n \leq 13$ for each genotype). (*C* and *D*) Col-0, *ap2m-1*, *twd40-2-3*, and *ap2m-1 twd40-2-3* plants are shown at 3 and 6 wk old. Thirty-three percent of *ap2m-1 twd40-2-3* mutants died at 3 wk. [Scale bars, 1 cm (*C*) and 5 cm (*D*).] (*E*) Western blot analysis of TWD40-2 expression in total protein extracts from Col-0, *ap2m-1*, *twd40-2-3*, *ap2m-1 twd40-2-3*, AP2M-YFP *ap2m-1*, and GFP-TWD40-2 *twd40-2-3* seedlings. TWD40-2 protein levels are reduced in seedlings harboring *twd40-2-3*. GFP-TWD40-2 *twd40-2-3* shows both knocked-down endogenous TWD40-2 and mobility-shifted GFP-TWD40-2. The loading control is a Coomassie gel.

To better understand the role of TWD40-2 in endocytosis and the functional relationship between TWD40-2 and the AP2 complex, *twd40-2-3* was crossed with *ap2m-1* (11). The double mutant, *ap2m-1 twd40-2-3*, exhibited enhanced dwarfism in etiolated hypocotyls, light-grown roots, and adult plants compared with *twd40-2-3*, and one-third of *ap2m-1 twd40-2-3* plants died ∼3 wk after germination (Fig. 1 *A*–*C*). The variation of phenotype was probably due to variation in the expression of *TWD40-2* and the gametophytic penetrance of *twd40-2-3* in the *ap2m-1* mutant background. In agreement with previous studies (11), qPCR and qualitative RT-PCR analysis confirmed that *ap2m-1* is a null allele (Fig. S1 *C* and *D*). The expression of *TWD40-2* was not significantly altered in a compensatory manner by *ap2m-1*, and AP2M transcription levels were not significantly altered in *twd40-2-3* (Fig. S1C). The severe growth defects of *ap2m-1 twd40-2-3* etiolated hypocotyls and light-grown roots represent a synergistic genetic interaction between *AP2M* and *TWD40-2*, because although *twd40-2-3* showed intermediately shortened hypocotyls and roots, *ap2m-1* single mutants displayed mildly elongated hypocotyls and roots. Together, the difference in phenotype between *ap2m-1* and *twd40-2-3* coupled with the synergistic phenotype displayed in *ap2m-1 twd40-2-3* seedlings suggests that AP2M and TWD40-2 probably undertake distinct yet cooperative roles in the process of clathrin-mediated endocytosis.

***ap2m-1*, *twd40-2-3*, and *ap2m-1 twd40-2-3* Have Unique and Varying Influences on Clathrin-Mediated Endocytosis.** To better understand the differences in the phenotypes of *ap2m-1*, *twd40-2-3*, and *ap2m-1 twd40-2-3* as well as the differences in the function of AP2M and TWD40-2 in endocytosis, an array of endocytosis efficiency experiments was performed in each of the genetic backgrounds. FM4-64 is a lipophilic fluorescent dye that is commonly used to label the plasma membrane and subsequently trace the route of endocytosed material in plant cells (20). After 8.5 min of exposure to 1 μM FM4-64, root meristematic epidermal cells of wild-type seedlings showed a strong labeling of the plasma membrane and exhibited labeling of many bright intracellular puncta that were representative of endocytosed material (Fig. S3). Under the same conditions, the endocytosis of FM4-64 in *ap2m-1*, *twd40-2-3*, and *ap2m-1 twd40-2-3* cells was significantly reduced compared with wild type (Fig. S3). The FM4-64 internalization defect of *twd40-2-3* was partially rescued by the expression of GFP-TWD40-2 (Fig. S3). In addition to the stark differences between the general endocytosis efficiency of wild-type and mutant seedlings exposed in the FM4-64 internalization experiments, a gradient of increasing endocytosis defect severity became apparent between *ap2m-1*, *twd40-2-3*, and *ap2m-1 twd40-2-3* (Fig. S3*B*).

Although the FM4-64 internalization assay is suitable for monitoring general endocytosis deficiencies, it is unable to probe how each mutation mechanistically influences CME. To directly observe CME events, a previously reported CLC-mOrange line was crossed with *ap2m-1*, *twd40-2-3*, and *ap2m-1 twd40-2-3* (19). Two populations of CLC are visible in spinning-disk confocal images of CLC-mOrange. CLC-mOrange localized to globular intracellular structures that have been previously identified as trans-Golgi network/early endosome (TGN/EE) compartments and to small, diffraction-limited particles at the PM that exhibit appearing and disappearing behavior, which is representative of the formation of clathrin-coated pits (CCPs) and scission of clathrin-coated vesicles (CCVs), respectively (Movie S1) (19, 21). Analysis of CLC-mOrange particles in this study was limited to

regions of interest that exclusively contained PM-localized CLC-mOrange particles as determined by the size and spatiotemporal behavior of the particles. The density of PM-localized CLC particles was significantly decreased in both *ap2m-1* and *ap2m-1 twd40-2-3* lines and insignificantly increased in *twd40-2-3* (Fig. 2 *A* and *B*). The resident lifetimes of PM-localized CLC-mOrange particles were slightly shortened in *ap2m-1* and drastically lengthened by *twd40-2-3* and *ap2m-1 twd40-2-3* (Fig. 2 *A* and *C* and Movie S1). Clearly, *ap2m-1* and *twd40-2-3* differentially influenced CLC behavior and *ap2m-1 twd40-2-3* shared characteristic effects of both *ap2m-1* and *twd40-2-3*, suggesting that AP2M and TWD40-2 each plays important, cooperative, and distinct roles in CME.

Because *ap2m-1* and *twd40-2-3* influenced the behavior of CLC in different ways, the turnover rate of PM-localized CLC-mOrange particles within a specified area was used as a unified metric for the overall efficiency of CME and compared among the mutants. Both *twd40-2-3* and *ap2m-1 twd40-2-3* exhibited significantly reduced rates of CLC-mOrange turnover (Fig. 2*D*). In contrast, despite the reduced density of CLC particles in *ap2m-1*, the reduction in turnover rates in *ap2m-1* was statistically insignificant due to the shortened lifetimes of CLC-mOrange particles in *ap2m-1* (Fig. 2*D*).

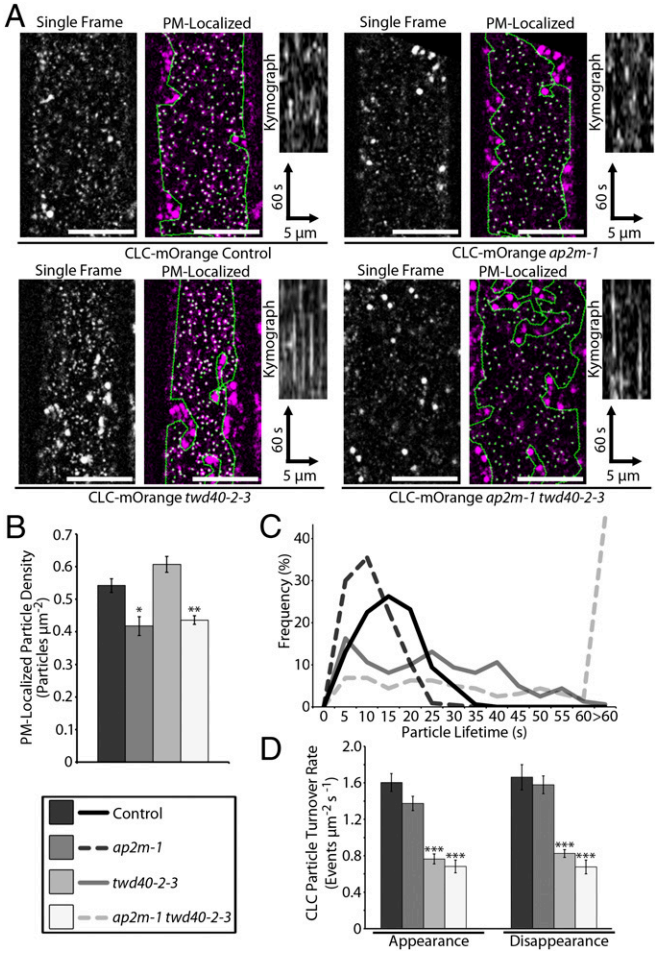

Fig. 2. PM-localized CLC-mOrange particles are differentially affected by *ap2m-1*, *twd40-2-3*, and *ap2m-1 twd40-2-3*. (*A*) A representative image of CLC-mOrange is displayed with and without automated particle detection of PM CLC particles in control, *ap2m-1*, *twd40-2-3*, and *ap2m-1 twd40-2-3* etiolated hypocotyls. (Scale bars, 10 μm.) Kymographs display particle dynamics over a 2-min time course. (*B*) Quantification of PM CLC particle densities. Error bars are SEM. $*P < 0.01$, $**P < 0.001$ ($n = 10$ for each genotype). (*C*) A histogram of PM CLC particle lifetimes ($n = 160$ particles from eight seedlings for each genotype). (*D*) The average CLC particle turnover rate is displayed as the rate of appearance and disappearance events per μm^2 per second. Error bars are SEM. $***P < 0.0001$ ($n = 10$ for each genotype).

An Increasing Severity of Endocytic Deficiency Correlates with Reduced Cellulose Biosynthesis by Influencing CESA Distribution and Dynamics. To investigate whether CME efficiency is important for maintaining efficient cellulose biosynthesis, the crystalline cellulose content was measured in each CME mutant background. Wild-type (Col-0) and *cesa6*$^{prc1-1}$ seedlings were used as controls for normal and deficient cellulose content, respectively (Fig. 3*A*). Although the cellulose content of *ap2m-1* seedlings was not significantly different from Col-0, *twd40-2-3* and *ap2m-1 twd40-2-3* each showed significant cellulose deficiencies of increasing severity (Fig. 3*A*), suggesting that CME defects can lead to inefficient cellulose biosynthesis.

To gain insight into the manner by which endocytic defects lead to cellulose biosynthesis defects, a YFP-CESA6 line that complements *cesa6*$^{prc1-1}$ was crossed into the *twd40-2-3* and *ap2m-1 twd40-2-3* genetic backgrounds. As previously observed, YFP-CESA6 in the control line localized to large globular Golgi bodies and to discrete, diffraction-limited particles at the PM (Fig. 3*B* and Movie S2) (5). The *ap2m-1* mutation was previously shown to cause an increase in the particle density of PM-localized YFP-CESA6 but did not significantly influence the dynamics of PM-localized YFP-CESA6 particles (11). An increase in PM-localized YFP-CESA6 particle density was also caused by *twd40-2-3* and *ap2m-1 twd40-2-3*, as indicated by the quantification of particle densities measured by automated particle detection within regions of interest that exclusively contained PM-localized YFP-CESA6 particles (Fig. 3 *B* and *C*). Interestingly, PM-localized YFP-CESA6 particle velocities were negatively influenced by *twd40-2-3* and *ap2m-1 twd40-2-3* compared with the control line, which correlates with the cellulose deficiency phenotypes of *twd40-2-3* and *ap2m-1 twd40-2-3* (Fig. 3 *A*, *B*, and *D* and Movie S2). The double mutant *ap2m-1 twd40-2-3* caused a more severe increase in particle density and a more severe decrease in CSC velocity than *twd40-2-3* alone. Approximately one-third of the YFP-CESA6 *ap2m-1 twd40-2-3 prc1-1* seedlings exhibited an abnormal YFP-CESA6 distribution in some epidermal cells. These abnormal cells had attributes that included a diffuse PM-localized YFP-CESA6 population that was extremely sensitive to photobleaching, faint PM-localized YFP-CESA6 particles, some MASC/SmaCC-like YFP-CESA6 compartments, and severely slowed or stalled cytoplasmic streaming (Movie S2). These abnormal cells were not included in the analysis of YFP-CESA6 density or dynamics.

The negative influence of *twd40-2-3* and *ap2m-1 twd40-2-3* on endocytosis, CESA function, and cellulose content revealed the importance of efficient CESA trafficking in the process of cellulose biosynthesis. To further corroborate the connection between intracellular trafficking and cellulose biosynthesis, we used an alternative means of CME disruption. Chemical induction of HUB1, a dominant-negative clathrin heavy chain (CHC) truncation, was previously shown to inhibit CME and arrest root elongation (22). In the HUB1 inducible line, INTAM>>RFP-HUB1, etiolated hypocotyl elongation inhibition was dependent on the concentration of the inducer, 4-hydroxytamoxifen (TAM) (Fig. S4*A*). HUB1 induction by 200 nM TAM caused a reduction of etiolated hypocotyl growth that was comparable to that of *ap2m-1 twd40-2-3* grown in normal conditions (Fig. S4*A*). Under HUB1 induction with 200 nM TAM, INTAM>>RFP-HUB1 seedlings exhibited a significant cellulose content deficiency, further emphasizing the influence of CME on cellulose biosynthesis (Fig. S4*B*). In controls, 200 nM TAM did not alter the cellulose content of Col-0 or *cesa6*$^{prc1-1}$ seedlings, and INTAM>>RFP-HUB1 etiolated hypocotyls grown in the absence of TAM had a normal cellulose content (Fig. S4*B*).

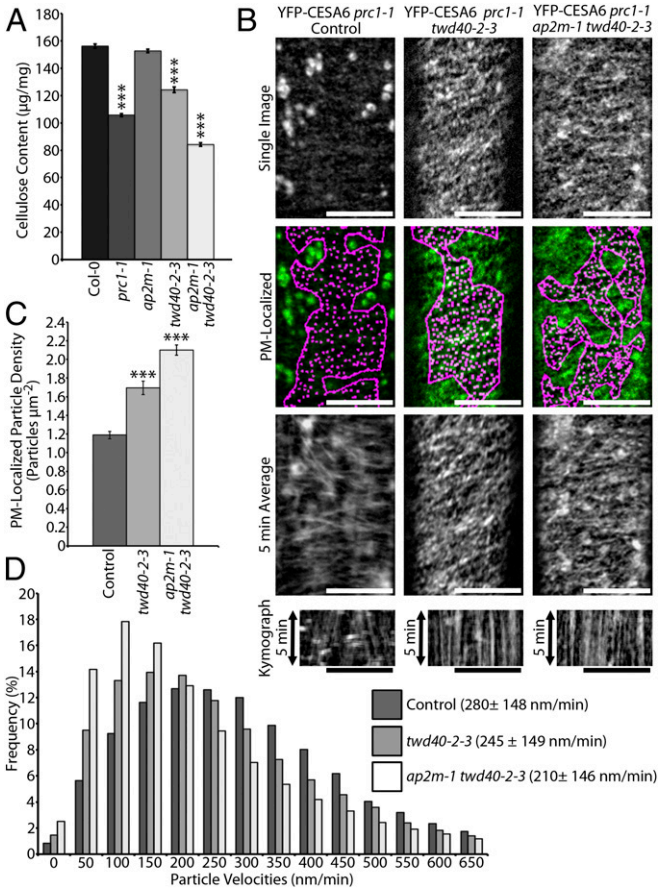

Fig. 3. Endocytic deficiencies of *twd40-2-3* and *ap2m-1 twd40-2-3* negatively influence cellulose biosynthesis by altering CESA distribution and dynamics. (*A*) The graph compares the crystalline cellulose content of 5-d-old etiolated seedlings of Col-0, *cesa6*$^{prc1-1}$, *ap2m-1*, *twd40-2-3*, and *ap2m-1 twd40-2-3*. Error bars are SEM. ***$P < 0.0001$ ($n = 10$ replicates per genotype). (*B*) A representative single-frame image of YFP-CESA6 is displayed in control (*cesa6*$^{prc1-1}$), *twd40-2-3*, and *ap2m-1 twd40-2-3* with and without automated particle detection of PM YFP-CESA6 particles. Corresponding time-averaged projections and kymographs show the trajectories and movement of PM YFP-CESA6 particles, respectively. (Scale bars, 10 μm.) (*C*) The average PM YFP-CESA6 particle density is quantified. Error bars are SEM. ***$P < 0.0001$ ($n \geq 20$ cells for each line). (*D*) The distribution and average of YFP-CESA6 velocities in each genetic background are displayed ($n \geq 19$ cells for each line). Averages are displayed ± SD.

TWD40-2 and AP2M Play Distinct but Associated Roles in CME. Although evidence suggests that AP2M and TWD40-2 are both involved in CME, *ap2m-1* and *twd40-2-3* mutants vary in the manner and magnitude by which they influence CME, endocytic cargo such as CESA, and cellular processes such as cellulose biosynthesis. A series of cell biology experiments was carried out to functionally position TWD40-2 within the CME process. To ascertain the spatiotemporal relationship among TWD40-2, AP2M, and CLC, we generated three dual-labeled lines, GFP-TWD40-2 CLC-mOrange, GFP-TWD40-2 AP2M-mCherry, and AP2M-YFP CLC-mOrange. In single-frame images, many colocalized particles were observed in each dual-labeled line (Fig. 4 *A*, *D*, and *G*); however, a particle often appeared or disappeared at a slightly different time point than its corresponding colocalized particle (Fig. 4 *B*, *E*, and *H* and Fig. S5). Therefore, colocalization analyses of single-frame images fail to represent the frequency of functional association between particles. Instead, each individual particle of interest was tracked temporally to assess whether a corresponding colocalized particle existed at any time during the lifetime of the particle of interest. Two particles were deemed to be functionally associated if they were spatiotemporally colocalized for at least two frames (for greater than 5 s) of live-cell imaging and only if colocalization was initiated by the appearance of a particle and terminated by the disappearance of a particle and not by the lateral diffusion of either particle. High frequencies of functional association were observed in each dual-labeled line, confirming that TWD40-2 cooperates with AP2M and predominantly participates in CME (Fig. 4 *C*, *F*, and *I*).

Furthermore, the dynamic relationship between each pair of functionally associated particles was recorded to determine whether a bias exists for the temporal order of appearance or disappearance among TWD40-2, AP2M, and CLC (Fig. 4 *C*, *F*, and *I*). AP2M showed a strong bias to appear before or at the same time

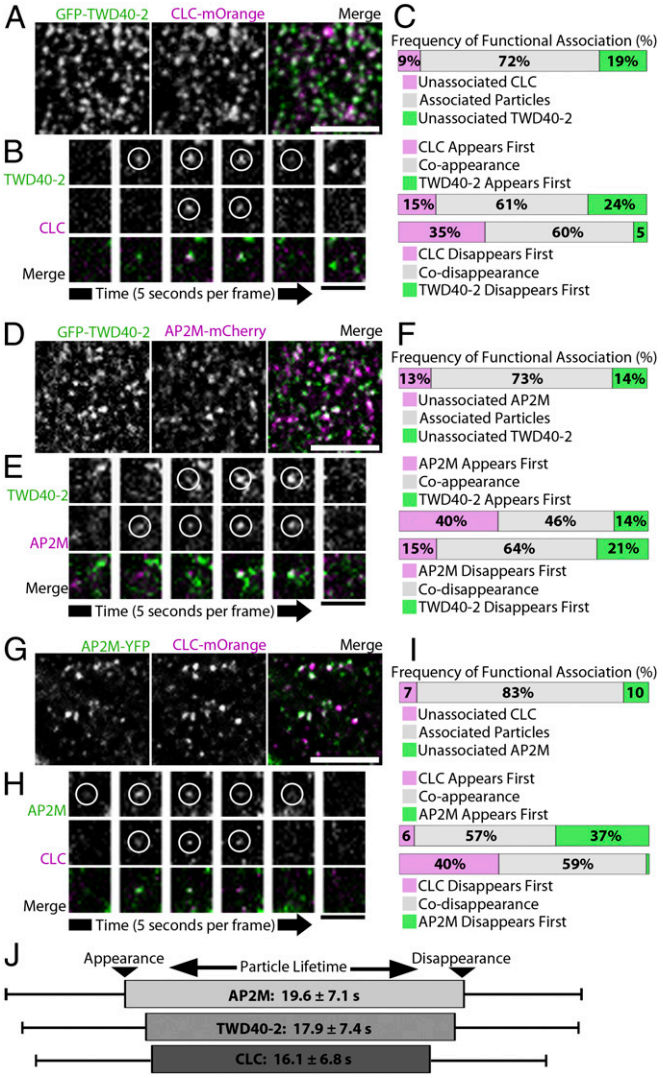

Fig. 4. TWD40-2, AP2M, and CLC are functionally associated. (*A*, *D*, and *G*) Single-frame images of GFP-TWD40-2/CLC-mOrange, GFP-TWD40-2/AP2M-mCherry, and AP2M-YFP/CLC-mOrange show colocalized particles. (Scale bars, 5 μm.) (*B*, *E*, and *H*) Representative time-lapse images show that functionally associated particles often appear or disappear at different time points during endocytic events. (Scale bars, 1 μm.) (*C*, *F*, and *I*) The frequency of functional association between particles was analyzed spatiotemporally over the entire lifetime of each particle. For each pair of functionally associated particles, the order of appearance and disappearance of the two particles was recorded ($n = 100$ observations, five seedlings for each line). (*J*) A schematic diagram shows the most likely sequence of appearance and disappearance of AP2M, TWD40-2, and CLC particles scaled to the average particle lifetimes of each protein. Error bars and ± values are SD ($n > 350$ particles, 26 seedlings for each protein).

as either TWD40-2 or CLC. Also, CLC showed a strong bias to disappear before or at the same time as either TWD40-2 or AP2M. Average particle lifetimes of each component were measured to be 19.6 ± 7.1 s for AP2M, 17.9 ± 7.4 s for TWD40-2, and 16.1 ± 6.8 s for CLC (Fig. 4*J*). These observations were used to develop a schematic diagram of CME that depicts the average particle lifetimes of each component and the most probable order of recruitment and dissociation of each component during CME (Fig. 4*J*). In this model, AP2M recruitment precedes that of TWD40-2 and CLC, whereas CLC dissociation precedes that of TWD40-2 and AP2M.

If AP2M and TWD40-2 are truly cooperating in CME, *ap2m-1* would influence TWD40-2 and *twd40-2-3* would influence AP2M. GFP-TWD40-2 particle density was significantly decreased in *ap2m-1*, similar to how *ap2m-1* influenced CLC-mOrange density (Fig. S6 *A* and *B* and Movie S3). However, unlike CLC-mOrange, which exhibited shortened particle lifetimes in *ap2m-1*, the lifetimes of GFP-TWD40-2 particles at the PM were relatively unchanged or lengthened in *ap2m-1* (Fig. S6 *A* and *C* and Movie S3). The converse experiment was also performed in which the effect of *twd40-2-3* on AP2M-YFP was analyzed. *twd40-2-3* did not affect the density of PM-localized AP2M-YFP particles, but did cause a severe increase in the lifetimes of AP2M-YFP particles (Fig. S6 *D–F* and Movie S3). The influence of *twd40-2-3* on AP2M was similar to its influence on CLC, but AP2M exhibited a more severe increase in particle lifetimes than CLC. These observations show that TWD40-2 and AP2M are codependent on each other and assume different roles in endocytosis.

Knowing that *ap2m-1* and *twd40-2-3* affect CME in different ways, we wondered whether inhibition of CME would likewise differentially influence AP2M and TWD40-2. The INTAM>>RFP-HUB1 line was crossed with GFP-TWD40-2 and AP2M-YFP, and CME inhibition was carried out by 24-h RFP-HUB1 induction with 2 μM TAM. To minimize the effect of induction-level variation, only seedlings with strong RFP-HUB1 induction were selected for analysis and compared against DMSO mock-treated seedlings from the same line that had no detectable RFP-HUB1 expression. Both AP2M-YFP and GFP-TWD40-2 were still recruited to discrete particles at the PM in the presence of strong RFP-HUB1 induction (Fig. S7 *A* and *B*). However, the lifetimes of these AP2M-YFP and GFP-TWD40-2 particles were extremely extended (Fig. S7*C* and Movie S4). These observations suggest that AP2M and TWD40-2 are early CME components that are recruited to the PM independent of a functional clathrin coat. However, the removal of AP2M and TWD40-2 from the PM is dependent on functional clathrin coats.

Discussion

The Cooperative and Distinct Functions of TWD40-2, the AP2 Complex, and the TPC in Clathrin-Mediated Endocytosis. The relatively mild phenotypes of AP2 mutants caused us to speculate that other AP complexes or proteins were redundant with AP2 in CME in *Arabidopsis* (11). As it turns out, the TPC could be the culprit for AP2 redundancy (17). Several lines of evidence suggest that AP2M and TWD40-2 cooperate in the process of CME. In animal cells, which lack homologs of the TPC and TWD40-2, the AP2 complex plays a crucial role in recruiting clathrin throughout the CME process (16). Accordingly, AP2 knockdown in animal cells caused a reduction in the density and an increase in the lifetimes of PM CLC particles due to reduced clathrin recruitment during CME initiation and maturation, respectively (23). In plants, although *ap2m-1* and *twd40-2-3* each impaired CME and influenced PM CLC particles independently, only the double mutant, *ap2m-1 twd40-2-3*, both reduced the density and increased the lifetimes of PM CLC particles, suggesting that AP2 and TWD40-2/TPC cooperate in plants to fulfill the function of the AP2 complex in animals. Further showing AP2M and TWD40-2 cooperation, both AP2M and TWD40-2 appeared early and persisted throughout CME in spatiotemporal analyses, suggesting that both proteins likely facilitate CME initiation, maturation, and scission (Fig. S8). The functions of AP2M and TWD40-2 were shown to be dependent on one another because *ap2m-1* altered GFP-TWD40-2 particles and *twd40-2-3* altered AP2M-YFP particles. AP2M and TWD40-2 were also similarly affected by HUB1 induction, under which AP2M and TWD40-2 particles were each recruited to stalled particles at the plasma membrane, suggesting that functional clathrin is required for the disengagement but not the recruitment of AP2M and TWD40-2 at the PM.

Several opposing characteristics of AP2M and TWD40-2 suggest that they play some distinct roles in CME. The contrast between the mildly lengthened etiolated hypocotyls of *ap2m-1* and dwarfed etiolated hypocotyls of *twd40-2-3* exemplifies the differences in AP2 and TWD40-2 mutant phenotypes. We hypothesize that these different growth phenotypes can be attributed to differences in the magnitude of CME deficiency in *ap2m-1* and *twd40-2-3*, which was reflected in the varying CLC-mOrange particle turnover rates of each mutant. For instance, cellular processes that are sensitive to trafficking perturbations may be affected to a smaller extent in *ap2m-1*, which has a mild CME deficiency, compared with *twd40-2-3*, which has a more severe CME deficiency, thereby leading to the different growth phenotypes.

The differences in the manner and magnitude of *ap2m-1* and *twd40-2-3* influences on CME components may help in hypothesizing the distinct attributes of AP2M and TWD40-2. Evidence suggests that CME initiation might be assumed by both AP2M and TWD40-2. The early recruitment of AP2M during CME and the reduced densities of CLC and TWD40-2 particles in *ap2m-1* implicate AP2M in CME initiation. In *ap2m-1*, TWD40-2/TPC may be able to assume the responsibilities of AP2 but operate at a reduced efficiency. Appropriately, GFP-TWD40-2 particles were still recruited to dynamic PM-localized particles in *ap2m-1*, but the density of TWD40-2 particles was reduced and the lifetimes of TWD40-2 particles were slightly extended. The involvement of TWD40-2 in CME initiation is supported by the significant reductions in the rate of appearance of CLC particles per μm^2 observed in *twd40-2-3*. The severely extended lifetimes of both CLC and AP2M particles in *twd40-2-3* suggest that TWD40-2 might play a distinct role in CME maturation or scission that cannot be assumed by AP2 (Fig. S8). A possible unique role of TWD40-2 in CME scission could involve the recruitment of dynamin-related proteins by TWD40-2 (Fig. S8). Alternatively, TWD40-2 could play a unique quality assurance "checkpoint" role during CME maturation that triggers faulty CME events to be aborted (Fig. S8). In other organisms, abortive CME events result in abbreviated CME particle lifetimes (24–26). In our study, *ap2m-1* had an elevated percentage of CLC particles with short lifetimes, which might be indicative of CME abortive events. In contrast, the extended CLC and AP2M lifetimes of *twd40-2-3* and *ap2m-1 twd40-2-3* could represent faulty CME events that are unable to abort. If *ap2m-1* has an increased incidence of abortive CME events, it is possible that the actual CME efficiency of *ap2m-1* is lower than our CLC particle turnover measurements suggest, which might be supported by the prominent FM4-64 internalization defect in *ap2m-1*.

Even if the AP2 complex, TWD40-2, and the TPC are all mechanistically similar to one another, different *ap2m-1* and *twd40-2-3* phenotypes could result from differences in cargo specificity or differences in the physical dimensions or integrity of CCVs with varying ratios of AP2 complexes, TWD40-2 proteins, and TPCs. Another interesting hypothesis is that TWD40-2 could act as a coat protein. The predicted structure of TWD40-2 has two β-propeller motifs followed by an extended α-solenoid region, which is a feature of the β′-COP subunit of the coat protein complex 1 (COPI) and is similar to many other vesicle coat proteins (18). Our data neither support nor refute the possibility of TWD40-2 acting as a coat protein in CME, but this proposition and the remaining mystique surrounding the TPC

are representative of the excitement and opportunity that exist in the study of plant endocytosis.

Cellulose Biosynthesis Relies on Efficient Endocytosis of CESA. We hypothesize that CSC endocytosis acts as a regulatory mechanism to maintain an organized distribution of productive CSCs at the PM. The directed delivery of CSCs along CMTs during exocytosis is evidence of organized CSC trafficking to the PM (6, 7). It seems likely that the endocytosis of CSCs is equally organized and regulated. CSCs with deficiencies in cellulose synthesis caused either by disengagement from the CMTs or by other means may be actively targeted for endocytosis. Once endocytosed, CSCs may either be recycled to the PM or directed for degradation, depending on the integrity of the CSC. We hypothesize that the severe endocytic deficiencies of *twd40-2-3* or *ap2m-1 twd40-2-3* lead to the excessive accumulation of these faulty CSCs at the PM. Consistent with this hypothesis, *twd40-2-3* and *ap2m-1 twd40-2-3* exhibited a reduced cellulose content, an increased density of PM CSCs, and a reduced velocity of PM CSCs which is indicative of the enzymatic inefficiency of faulty CSCs. In *ap2m-1*, which has a milder endocytic deficiency, CSC overaccumulation still occurs, but low levels of endocytosis may still adequately remove many faulty CSCs from the PM, resulting in higher PM CSC density without significantly influencing PM CSC velocities. The inverse relationship between the density of PM-localized CSCs and cellulose content and the direct relationship between CSC velocities and cellulose content in *ap2m-1*, *twd40-2-3*, and *ap2m-1 twd40-2-3* suggest that the quality of PM-localized CSCs is more influential for cellulose biosynthesis than the sheer abundance of PM-localized CSCs, and that CME can influence CSC quality in addition to CSC quantity at the PM.

In this study, CESA and cellulose biosynthesis represent just a single cargo protein and a single cellular process that is influenced by regulated endocytosis. A broader understanding of both the mechanisms and cargo specificities of plant CME machinery components is sure to underscore the importance of regulated CME in many other processes in the future. Plants offer the opportunity to characterize the functions of rarely conserved TPC machinery that may provide insight into the evolution of trafficking machinery of all eukaryotes.

Materials and Methods

Plant Materials. *SALK_112497* (*twd40-2-3*) was obtained from the *Arabidopsis* Biological Resource Center (ABRC) at Ohio State University. The *ap2m-1* (previously referred to as *μ2-1*) and AP2M-YFP (previously referred to as μ2-YFP) lines were previously described (11). The YFP-CESA6, CLC-mOrange, and INTAM>>RFP-HUB1 lines were also previously described (5, 19, 22). The GFP-TWD40-2 *twd40-2-3* line was constructed with a 2-kb native TWD40-2 promoter region using the primers in Table S1.

See *SI Materials and Methods* for details on the construction, genotyping, and expression analysis of the transgenic and mutant lines.

Live-Cell Imaging and Analysis. With the exception of two experiments (FM4-64 internalization assay and imaging under HUB1 induction), all images were obtained of epidermal cells 1–2 mm below the apical hook of 3-d-old etiolated hypocotyls.

See *SI Materials and Methods* for details on dye treatment, induction conditions, and image analysis.

Cellulose Content Analysis. The crystalline cellulose content was measured by the Updegraff method (27).

See *SI Materials and Methods* for details.

ACKNOWLEDGMENTS. We thank S. Bednarek for providing the CLC-mOrange line, J. Friml for the INTAM>>RFP-HUB1 line, and C. R. Somerville for the YFP-CESA6 line. We also thank Deborah Grove and the Penn State Genomics Core Facility for aiding us in designing and conducting the real-time qPCR experiments. This work was supported by the Center for Lignocellulose Structure and Formation, an Energy Frontier Research Center funded by the US Department of Energy, Office of Science, Basic Energy Sciences, under Award DE-SC0001090.

1. Cosgrove DJ (2005) Growth of the plant cell wall. *Nat Rev Mol Cell Biol* 6(11):850–861.
2. Somerville C (2006) Cellulose synthesis in higher plants. *Annu Rev Cell Dev Biol* 22: 53–78.
3. Bashline L, Li S, Gu Y (2014) The trafficking of the cellulose synthase complex in higher plants. *Ann Bot (Lond)* 114(6):1059–1067.
4. Li S, Bashline L, Lei L, Gu Y (2014) Cellulose synthesis and its regulation. *Arabidopsis Book* 12:e0169.
5. Paredez AR, Somerville CR, Ehrhardt DW (2006) Visualization of cellulose synthase demonstrates functional association with microtubules. *Science* 312(5779):1491–1495.
6. Crowell EF, et al. (2009) Pausing of Golgi bodies on microtubules regulates secretion of cellulose synthase complexes in *Arabidopsis*. *Plant Cell* 21(4):1141–1154.
7. Gutierrez R, Lindeboom JJ, Paredez AR, Emons AMC, Ehrhardt DW (2009) *Arabidopsis* cortical microtubules position cellulose synthase delivery to the plasma membrane and interact with cellulose synthase trafficking compartments. *Nat Cell Biol* 11(7): 797–806.
8. Gu Y, et al. (2010) Identification of a cellulose synthase-associated protein required for cellulose biosynthesis. *Proc Natl Acad Sci USA* 107(29):12866–12871.
9. Lei L, Li S, Du J, Bashline L, Gu Y (2013) Cellulose synthase INTERACTIVE3 regulates cellulose biosynthesis in both a microtubule-dependent and microtubule-independent manner in *Arabidopsis*. *Plant Cell* 25(12):4912–4923.
10. Li S, Lei L, Somerville CR, Gu Y (2012) Cellulose synthase interactive protein 1 (CSI1) links microtubules and cellulose synthase complexes. *Proc Natl Acad Sci USA* 109(1): 185–190.
11. Bashline L, Li S, Anderson CT, Lei L, Gu Y (2013) The endocytosis of cellulose synthase in *Arabidopsis* is dependent on μ2, a clathrin-mediated endocytosis adaptin. *Plant Physiol* 163(1):150–160.
12. Di Rubbo S, et al. (2013) The clathrin adaptor complex AP-2 mediates endocytosis of brassinosteroid insensitive1 in *Arabidopsis*. *Plant Cell* 25(8):2986–2997.
13. Fan L, et al. (2013) Dynamic analysis of *Arabidopsis* AP2 σ subunit reveals a key role in clathrin-mediated endocytosis and plant development. *Development* 140(18):3826–3837.
14. Kim SY, et al. (2013) Adaptor protein complex 2-mediated endocytosis is crucial for male reproductive organ development in *Arabidopsis*. *Plant Cell* 25(8):2970–2985.
15. Yamaoka S, et al. (2013) Identification and dynamics of *Arabidopsis* adaptor protein-2 complex and its involvement in floral organ development. *Plant Cell* 25(8):2958–2969.
16. McMahon HT, Boucrot E (2011) Molecular mechanism and physiological functions of clathrin-mediated endocytosis. *Nat Rev Mol Cell Biol* 12(8):517–533.
17. Gadeyne A, et al. (2014) The TPLATE adaptor complex drives clathrin-mediated endocytosis in plants. *Cell* 156(4):691–704.
18. Hirst J, et al. (2014) Characterization of TSET, an ancient and widespread membrane trafficking complex. *eLife* 3:e02866.
19. Konopka CA, Backues SK, Bednarek SY (2008) Dynamics of *Arabidopsis* dynamin-related protein 1C and a clathrin light chain at the plasma membrane. *Plant Cell* 20(5): 1363–1380.
20. Bolte S, et al. (2004) FM-dyes as experimental probes for dissecting vesicle trafficking in living plant cells. *J Microsc* 214(Pt 2):159–173.
21. Ito E, et al. (2012) Dynamic behavior of clathrin in *Arabidopsis thaliana* unveiled by live imaging. *Plant J* 69(2):204–216.
22. Kitakura S, et al. (2011) Clathrin mediates endocytosis and polar distribution of PIN auxin transporters in *Arabidopsis*. *Plant Cell* 23(5):1920–1931.
23. Boucrot E, Saffarian S, Zhang R, Kirchhausen T (2010) Roles of AP-2 in clathrin-mediated endocytosis. *PLoS One* 5(5):e10597.
24. Aguet F, Antonescu CN, Mettlen M, Schmid SL, Danuser G (2013) Advances in analysis of low signal-to-noise images link dynamin and AP2 to the functions of an endocytic checkpoint. *Dev Cell* 26(3):279–291.
25. Cocucci E, Aguet F, Boulant S, Kirchhausen T (2012) The first five seconds in the life of a clathrin-coated pit. *Cell* 150(3):495–507.
26. Loerke D, et al. (2009) Cargo and dynamin regulate clathrin-coated pit maturation. *PLoS Biol* 7(3):e57.
27. Updegraff DM (1969) Semimicro determination of cellulose in biological materials. *Anal Biochem* 32(3):420–424.
28. Karimi M, Inze D, Depicker A (2002) GATEWAY vectors for Agrobacterium-mediated plant transformation. *Trends Plant Sci* 7(5):193–195.
29. Livak KJ, Schmittgen TD (2001) Analysis of relative gene expression data using real-time quantitative PCR and the 2(-Delta Delta C(T)) Method. *Methods* 25(4):402–408.